[6] Chang, J., "Supersonic Molecular Beam Sampling Systems for Mass Spectrometri Studies of High Pressure Flow Systems," Research Rept. 326, April 1969, Avco Everett Research Lab., Everett, Mass.
[7] Laufer, J., "Turbulent Shear Flows of Variable Density," *AIAA Journal*, Vol. 7, No. 4, April 1969, pp. 706–713.
[8] Demetriades, A. and Doughman, E. L., "Mean and Intermittent Flow of a Self-Perserving Plasma Jet," *AIAA Journal*, Vol. 7, No. 4, April 1969, pp. 713–722.
[9] O'Conner, T. J., Comfort, E. H., and Cass, L. A., "Turbulent Mixing of an Axisymmetric Jet of Partially Dissociated Nitrogen with Ambient Air," *AIAA Journal*, Vol. 4, No. 11, Nov. 1966, pp. 2026–2032.
[10] Sutton, E., "The Chemistry of Electrons in Pure Air Hypersonic Wakes," *AIAA Journal*, Vol. 6, No. 10, Oct. 1968, pp. 1873–1883; also Research Rept. 266, July 1967; Avco Everett Research Lab., Everett, Mass.

DECEMBER 1973 AIAA JOURNAL VOL. 11, NO. 12

Nonequilibrium Flow Calculations for the Hydrogen Constricted Arc

ROBERT K. SCOTT* AND FRANK P. INCROPERA†
Purdue University, West Lafayette, Ind.

A nonequilibrium flow model has been formulated and solved numerically for conditions in an atomic hydrogen cascade arc. Solutions show that although thermal nonequilibrium effects are minor, the departure from chemical equilibrium is significant. Comparisons with results obtained from an equilibrium flow model reveal the deficiencies associated with such a model and parametric calculations reveal the effect of current, pressure, and radius on arc behavior.

Nomenclature

E = electric field intensity
I = arc current
I_p = ionization potential
k = Boltzmann's constant
n_e = electron number density
$\dot{n}_e$ = electron production rate
n_H = hydrogen atom number density
p = static pressure
P_I = diffusion of ionization energy
P_{rad} = radiative emission
q_{rad} = radiative wall heat flux
q_e = electron heat conduction
q_h = heavy particle heat conduction
q_w = total wall heat flux
R = tube radius
r = radial coordinate
S_{ec} = elastic collision energy transfer between electrons and heavy particles
T_e = electron temperature
T_h = heavy particle temperature
v_{amb} = ambipolar diffusion velocity
α_{rr} = radiative recombination coefficient
β = electron reflection coefficient
χ = ion reflection coefficient
σ_e = electrical conductivity

Introduction

THE wall stabilized cascade arc has been used extensively for the determination of high-temperature gas transport properties, for the simulation of high-speed aerodynamic phenomena, as a radiation source for photochemical processing, and as a means of energizing gas dynamic lasers. In support of these applications, much has been done to determine the thermochemical state of the arc gas. Earlier efforts involved the use of equilibrium flow models to predict arc temperature and species concentration profiles, as well as over-all heat-transfer effects.[1-3] More recently, however, comparisons between the equilibrium predictions and spectroscopic temperature measurements,[4,5] as well as comparisons with electric field intensity and wall heat-transfer data,[6] have suggested the existence of nonequilibrium effects. In particular, these comparisons have suggested the existence of a thermal nonequilibrium, for which there is a nonequipartition of translational energy between the electrons and heavy particles (each characterized by a separate kinetic temperature), and a chemical nonequilibrium, for which the Saha equation fails to predict species concentrations. Accordingly, more recent efforts to predict flow conditions in the cascade arc have considered the influence of thermochemical nonequilibrium conditions.[7-10]

The purpose of this study is to predict the thermochemical properties of the hydrogen arc and the extent to which nonequilibrium effects influence these properties. The behavior of hydrogen at elevated temperatures has astrophysical significance and bears directly on the simulation of Jupiter entry conditions.

Mathematical Model

Although conditions have been considered for both the entrance and asymptotic arc regions,[11] attention will be focused on the asymptotic results. In the asymptotic region, thermochemical conditions are uncoupled from hydrodynamic effects, and for prescribed arc operating conditions, the thermochemical variables depend only upon radius. It is assumed that the flow is laminar, steady, and axisymmetric, and that the electric field is directed only in the axial direction. The plasma is assumed to be quasineutral and is viewed as a perfect gas mixture of electrons, hydrogen ions, and neutral hydrogen atoms. The effect of neglecting the molecular species will be discussed later.

The governing differential equations may be derived by applying mass and energy conservation requirements to the

Received April 23, 1973; revision received July 18, 1973. Supported by NASA under Grant NGR 15-005-129.
Index category: Plasma Dynamics and MHD.
* Graduate Student.
† Professor. Member AIAA.

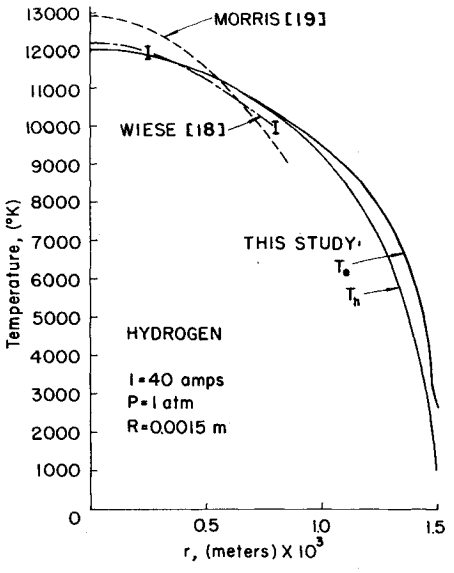

Fig. 1 Comparison of theoretical and experimental temperature distributions for a 40-amp, 0.0015-m radius hydrogen arc.

electron subgas and to the heavy particles. The appropriate equations are then

$$(1/r)\,d(rn_e v_{amb})/dr = \dot{n}_e \tag{1}$$

$$\frac{5}{2}\frac{k}{r}\frac{d(rn_e v_{amb} T_e)}{dr} = -\frac{1}{r}\frac{d(rq_e)}{dr} + \sigma_e E^2 + S_{ec} - P_{rad} - P_I \tag{2}$$

$$0 = -(1/r)\,d(rq_h)/dr - S_{ec} \tag{3}$$

$$p = n_e k(T_e + T_h) + n_h k T_h \tag{4}$$

Equations (1–4) are, respectively, the electron continuity and energy equations, the heavy-particle energy equation, and the thermal equation of state. The dependent variables are the electron and neutral atom number densities and the electron and heavy particle temperatures.

The methods used to determine the required transport and reaction rate coefficients are discussed in detail by Scott[11] and are summarized as follows. The ambipolar diffusion velocity and the electron and heavy particle heat conduction effects are expressed in terms of nonequilibrium transport coefficients and appropriate gradients. Mean-free-path models are then used to compute these transport coefficients, as well as the nonequilibrium electrical conductivity. To determine the accuracy of this procedure the nonequilibrium transport coefficients are evaluated in the limit of equilibrium and are compared with results obtained from a rigorous application of the methods of kinetic theory.[12] Although agreement between the two sets of results is in general good, multiplicative factors are assigned to the mean-free-path models to force agreement to within 10%. These factors assume values of 1.2, 3.0, and 1.0 for the ambipolar diffusion coefficient, the thermal conductivity, and the electrical conductivity, respectively.

The source term in the electron continuity equation includes electron production due to collisional ionization, three-body recombination, and radiative recombination. The three-body recombination coefficient is obtained from the data of Hinnov and Hirschberg,[13] and the electron ionization rate coefficient is obtained through detailed balancing. The radiative recombination coefficient, α_{rr}, is taken from Allen,[14] and the elastic energy exchange rate between electrons and heavy particles is computed from the model due to Petschek and Byron.[15] The contribution of radiative recombination to the radiative emission rate is computed using the product $C_1\alpha_{rr}n_e^2(I_p+3/2kT_e)$. The quantity C_1 is a correction factor used to force agreement of this model with results obtained in the limit of equilibrium. In particular, the radiative emission rate predicted by the model is compared with the results of Yos,[16] and a value of $C_1 = 0.4$ is needed to obtain agreement. The contribution of Bremsstrahlung to the radiative emission is computed from the method described by Longmire.[17] Finally, the term which accounts for the diffusion of ionization energy is computed from the product of the ionization potential and the electron production rate.

Boundary conditions are specified at the wall and the arc centerline. From the assumption of axisymmetric flow, all gradients must be zero at the centerline. At the wall, the heavy particle temperature is assumed to be fixed at 1000°K. However, to obtain appropriate conditions for the unknown electron number density and temperature at the wall, the presence of the wall electrostatic sheath must be considered. By performing mass and energy balances for the sheath, expressions for the electron particle and energy fluxes are obtained.[11] These may then be used as boundary conditions for the electron continuity and energy equations. Electron and ion wall reflection coefficients appear in the sheath equations and are used to characterize wall catalytic effects.

Due to the strong coupling and the presence of highly nonlinear terms in the governing equations, exact solutions cannot be obtained. Therefore, finite-difference techniques must be utilized if the rigor of the mathematical model is to be retained. Due to the large computer time required in the numerical solution of "stiff" equations, the number of grid points used in the finite-difference scheme must be minimized. For this reason, variable grid spacing is used with centerline spacing six times greater than at the wall. Since the resulting difference equations are transcendental, they cannot be solved simultaneously. Hence, the Newton-Raphson (iterative) method is used. The first estimate of dependent variables required to initiate the iterative procedure is obtained from either a flow solution for different arc operating conditions or from a finite-difference solution to the governing equations for the entrance region. Details of the numerics are provided by Scott.[11]

Results and Conclusions

Parameters of the hydrogen cascade arc which can be specified independently in the numerical solution are current (I), pressure (p), tube radius (R) and the electron and ion reflection coefficients (β and χ). A solution for the asymptotic arc region consists of obtaining the values of n_e, n_H, T_e, and T_h at every grid point, calculating the electric field intensity, and computing the various heat fluxes. Solutions are obtained for the purpose of comparing

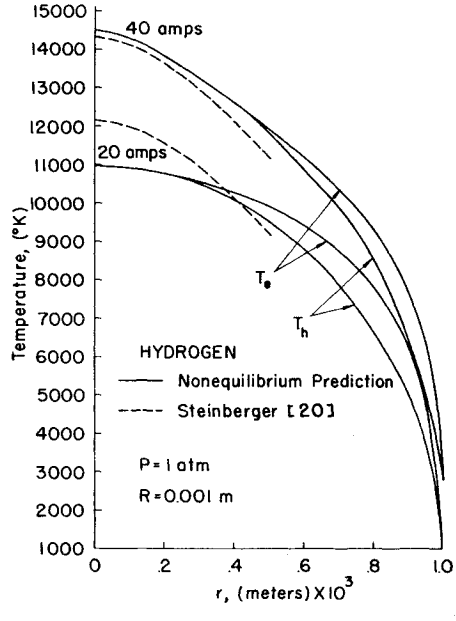

Fig. 2 Comparison of theoretical and experimental temperature distributions for a 0.001-m radius hydrogen arc.

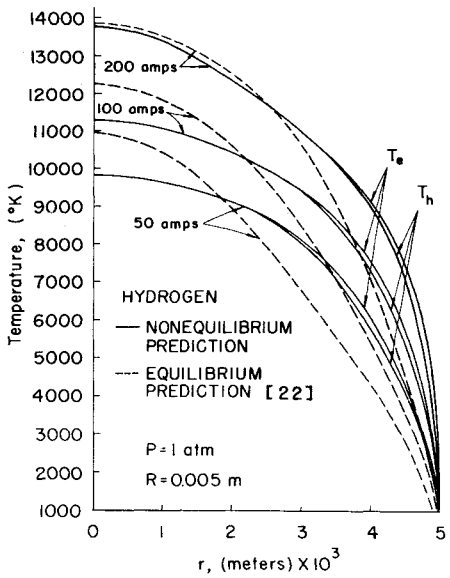

Fig. 3 Comparison of temperature profiles for equilibrium and nonequilibrium hydrogen cascade arcs.

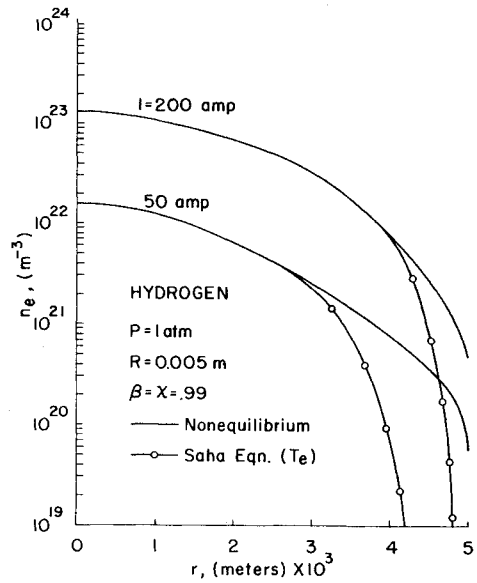

Fig. 4 Current dependence of chemical nonequilibrium.

both with available data and with corresponding equilibrium predictions. In addition, parametric calculations are performed to determine the effect of arc operating parameters on the thermochemical state of the gas. The range of conditions considered includes $20 \leqq I \leqq 200$ amp, $1 \leqq p \leqq 10$ atm, and $5 \times 10^{-3} \leqq R \leqq 5 \times 10^{-2}$ m.

In Figs. 1 and 2 the nonequilibrium temperature profiles of this study are compared with experimental profiles obtained for comparatively low values of R and I. In Fig. 1, the results of Wiese[18] were obtained from the measurement of Balmer line intensities and those by Morris,[19] from measurement of the continuum radiation. However, since the continuum measurements are thought to be obscured by several molecular processes and the presence of weak, highly broadened, impurity lines, the agreement between theory and experiment (the Wiese results) is viewed as good. The results of Steinberger[20] (Fig. 2) were obtained from the measurement of Balmer line intensities. Although the agreement between results is good at 40 amp, it is less satisfactory at 20 amp. This low current disparity is possibly due to convergence problems inherent in the numerical scheme when used at extremely low currents.

The equilibrium predictions of Greene[22] for the atomic hydrogen arc are compared with those of this study in Fig. 3. The lower equilibrium temperatures in the wall region are due to equilibrium electron densities which are many orders of magnitude lower than the nonequilibrium number densities. Since the equilibrium electrical conductivity is therefore much smaller than the nonequilibrium value, the equilibrium Ohmic heating term, $\sigma_e E^2$, and hence the local temperature, is greatly underpredicted in the wall region. The disparity between equilibrium and nonequilibrium predictions for the arc core may also be attributed to nonequilibrium effects. With increasing current, equilibrium is more closely approached in the arc core and the agreement between the equilibrium and nonequilibrium profiles improves.

A significant feature of Fig. 3 is the fact that the electron and heavy particle temperatures are very close to each other. Even at the wall the two species temperatures do not deviate by a great deal [$T_e(R) = 1936$°K for $I = 200$ amp and $T_e(R) = 1260$°K for $I = 50$ amp]. These results are due to the small mass of the hydrogen atom and suggest that equipartition of translational energy is achieved to an excellent approximation throughout the hydrogen arc. This is in contrast to results obtained for the Ar arc,[10] wherein T_e is frozen at values in excess of 7000°K near the wall.

In Fig. 4 the nonequilibrium electron number density is compared with the electron number density computed from the Saha equation evaluated at T_e. Although chemical equilibrium exists in the arc core, the departure from this condition is severe near the wall. This effect is due to a net ambipolar diffusion of charged particles to the wall in the absence of recombination rates sufficient to maintain equilibrium condi-

Table 1 Predicted and measured electric field intensities for the hydrogen arc

			E (v/m)				
I, amp	p, atm	R, m	Nonequilibrium	Maecker[21]	Wiese[18]	Morris[19]	Equilibrium[22]
20	1	0.0010	5572	12000	...	...	...
40	1	0.0010	5261	9800	...	...	...
50	1	0.0010	...	9000	...	...	...
20	1	0.0015	4040	...	...	9300	...
30	1	0.0015	3779	...	...	7400	...
40	1	0.0015	3672	...	5600	6800	...
50	1	0.0015	3617	...	...	6200	...
50	1	0.0050	1343	...	...	...	1824
100	1	0.0050	1200	...	...	...	1468
150	1	0.0050	1191	...	...	...	1375
200	1	0.0050	1223	...	...	...	1348

tions. Moreover, due to a decrease in the rate of equilibrium restoration (recombination) processes, the extent of the chemical nonequilibrium domain increases with decreasing current.

Note that the nonequilibrium predictions of Fig. 4 pertain to values of β and χ (the electron and ion sheath reflection coefficients) of 0.99. Parametric calculations were performed to determine the sensitivity of the nonequilibrium predictions to assumed values of these reflection coefficients. Values of β and χ were allowed to vary in the range from 0.99 to 0.0, and with the exception of a small region ($\Delta r < 10^{-4}$ m) adjoining the wall, the effect on the temperature and concentration profiles is negligible. At the wall T_e may vary by as much as 3000°K and n_e by an order of magnitude, according to the choice of β and χ. The effect of β and χ on the over-all electrical and heat-transfer properties is negligible. All results in this article are presented for β and χ fixed at 0.99.

Comparisons of the nonequilibrium predictions of electric field intensity with available data and equilibrium predictions are summarized in Table 1. Although the agreement between the experimental results and the nonequilibrium predictions improves with increasing current, it is poor over the range of currents for which data is available ($20 \leqq I \leqq 50$ amp). Although the disparity may be due in part to neglecting the molecular species and to uncertainties in the required properties, it may also be due to convergence errors in the numerical scheme which are incurred at low tube radii and arc currents. For similar temperature and number density profiles, the convergence error of the second order finite-difference operator is inversely proportional to the tube radius. This effect was confirmed through a convergence check which involves satisfying an over-all arc energy balance. For a five-fold increase in tube radius, the discrepancy in the energy balance was reduced from 15% to 1%. Although no data could be found for verification of the predictions at higher currents and radii, the convergence checks are satisfactory (e.g., at $I = 100$ amp and $R = 0.005$ m), and it is felt that parametric calculations may be effected with confidence.

Nonequilibrium and equilibrium predictions of the hydrogen arc field intensity are compared in Table 1 and Fig. 5. The agreement between the two prediction schemes is satisfactory, and the small discrepancy may be attributed to nonequilibrium effects. Note that, in the limit of equilibrium, the nonequilibrium and equilibrium models are based upon the same transport properties. Results obtained previously for argon are presented for comparison. The difference between the hydrogen and argon results is due largely to differences in the electrical conductivity,

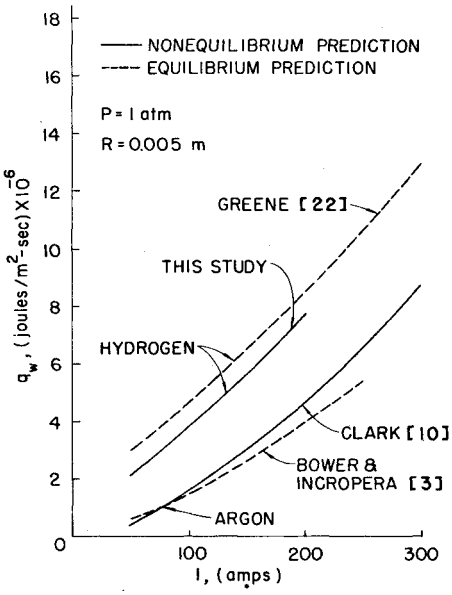

Fig. 6 Equilibrium and nonequilibrium calculations of total wall heat flux as a function of current in hydrogen and argon.

with the value for Ar generally exceeding that for H at a given current and point in the arc.

Comparative values for the total wall heat flux, Fig. 6, must exhibit the same trends as the field intensity, since the wall heat flux is equivalent to the product $E \cdot I$ in the asymptotic region. It should be noted, however, that of the various mechanisms which may contribute to the wall heat flux, only the contributions due to heavy-particle conduction and radiation are significant. Unlike the situation which exists for the Ar arc,[10] the "diffusion of ionization energy" was found to be negligible for the range of conditions considered.

The fraction of the total wall heat flux due to radiation is also of interest. Nonequilibrium and equilibrium predictions for the variation of this quantity with current are shown in Fig. 7 for the hydrogen and argon arcs. Although for hydrogen the equilibrium and nonequilibrium ratios are in good agreement, the magnitude of the equilibrium radiative flux exceeds the nonequilibrium value by 35% at 50 amp and by 4% at 200 amp. The reason for this disparity is apparent from the temperature

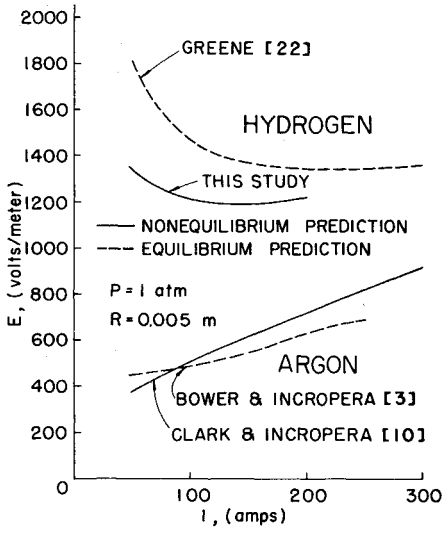

Fig. 5 Equilibrium and nonequilibrium calculations of electric field current characteristic in hydrogen and argon.

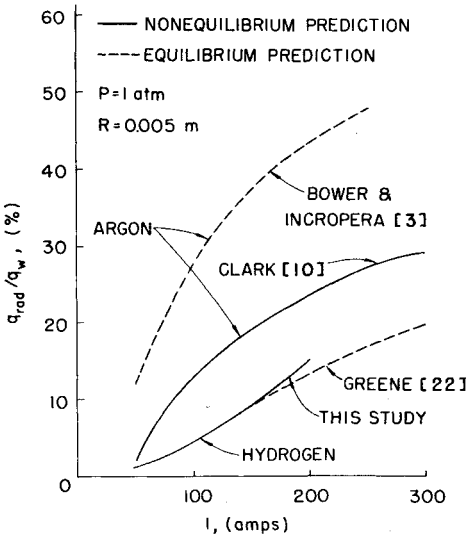

Fig. 7 Equilibrium and nonequilibrium calculations of radiative wall heat flux fraction as a function of current in hydrogen and argon.

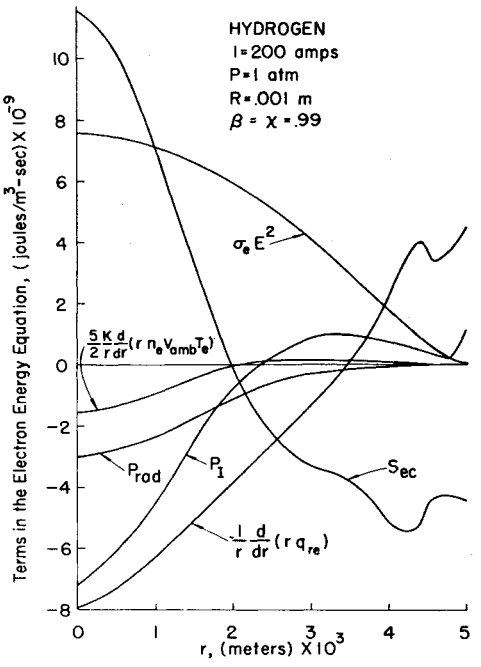

Fig. 8 Terms in the electron energy equation.

profiles of Fig. 3. Since the volumetric emission is a strong function of temperature, the higher temperatures predicted by the equilibrium model in the core of the low current arc result in higher values for the radiative wall flux. Note that for the hydrogen arc, the percent contribution of heavy-particle conduction to the wall heat flux is approximately 100 minus the results of Fig. 7. Note also that, although the equilibrium and nonequilibrium radiative flux fractions do not agree well for argon, the nonequilibrium predictions are in excellent agreement with data.[10] The radiative fraction for argon exceeds that for hydrogen due to the significantly higher electron concentrations and temperatures in the arc periphery.

Parametric calculations have been performed to determine the influence of current, pressure, and radius on arc performance. The effects of current are illustrated in Figs. 3–7 and the effects of pressure and radius are discussed in detail by Scott.[11] With increasing pressure the electron and heavy particle temperatures converge, temperatures in the arc core decrease, the electron number density increases, and chemical equilibrium conditions are more closely approached. Moreover, the electric field intensity (and hence the total wall heat flux) increases with increasing pressure. The relative contribution of radiation to the wall heat flux also increases significantly, achieving a value of 55% at $I = 200$ amp and $p = 10$ atm.

With increasing tube radius, the electron and heavy-particle temperatures converge and there is a general reduction of these temperatures as well as the electron number density. However, chemical nonequilibrium effects become more pronounced. With increasing radius, the electric field intensity (and hence the total wall heat flux) decreases. Although the radiative wall heat flux also decreases, there is little change in the relative contribution of radiation to the total flux.

With regard to the processes which influence arc energetics, it is instructional to compare the terms appearing in Eq. (2). Results are shown in Fig. 8, where positive values indicate energy transfer to the electron gas and negative values indicate transfer from this gas. As expected, the Ohmic heating term supplies energy to the electron gas over the entire cross section and radiative emission depletes the electron energy, particularly in the arc core. The diffusion of ionization energy, P_I, is negative in the arc core, since there is a net production of electrons in this region, and positive in the arc periphery due to a net consumption of electrons. Note also that there is a net loss of thermal energy due to ambipolar diffusion and conduction at points in the arc core and a net gain due to these processes in the arc periphery. The positive value of the elastic energy exchange term, S_{ec}, in the arc core is due to the fact that T_h is slightly higher (approximately 0.05%) than T_e. The large value of S_{ec} is due to the large electron number densities and electron-heavy particle collision frequencies characteristic of core conditions.

In this study, approximate theories have been used to represent the nonequilibrium transport properties, and due to the uncertainties associated with these representations, it is useful to determine their effect on the predictions of interest. Parametric calculations were performed in which the transport coefficients were varied by appropriate amounts (by as much as 250% for the radiative recombination coefficient and by as little as 25% for the thermal conductivity). The temperatures, electron concentrations, field intensity, and radiation flux were found to vary by less than 10, 40, 10 and 50%, respectively.

Although attention has been restricted to the atomic hydrogen arc, it is possible to infer how conditions might be altered by the presence of molecular hydrogen. Temperatures and electron concentrations would be lower due to added dissociation requirements; however this effect should only be pronounced near the wall. This should in turn promote a slightly larger field intensity, a lower radiation flux, and, together with the larger particle mass, an increased degree of thermal nonequilibrium. Despite these effects, however, the present solution is thought to provide reasonable estimates of both the over-all arc properties and the local properties in the arc core.

Summary

A nonequilibrium model has been formulated for conditions in an atomic hydrogen arc, and the key results are summarized as follows.

a) Thermal nonequilibrium effects are minor for the operating conditions of this study. Although chemical nonequilibrium is never significant near the tube centerline, it always exists in the wall region. The relative radial location (r/R) marking the onset of chemical nonequilibrium increases with increasing current, increasing pressure, and decreasing radius.

b) The major contributions to the wall heat flux are made by heavy-particle conduction and radiation. The contributions due to electron conduction and the diffusion of ionization energy are negligible.

c) An equilibrium description of arc behavior significantly underpredicts temperatures and electron concentrations near the wall and overpredicts the electric field intensity and the total and radiative wall heat fluxes. These effects diminish with increasing current and pressure.

It should be noted that the foregoing conclusions are based to a large degree on comparisons between two theories (equilibrium and nonequilibrium). The conclusions should therefore be regarded as tentative, pending the availability of additional data for the hydrogen arc.

References

[1] Stine, H. A. and Watson, V. R., "The Theoretical Enthalpy Distribution of Air in Steady Flow Along the Axis of a Direct-Current Electric Arc," TN D-1331, 1962, NASA.

[2] Watson, V., "Comparison of Detailed Numerical Solutions with Simplified Theories for the Characteristics of the Constricted-Arc Plasma Generator," *Proceedings of the 1965 Heat Transfer and Fluid Mechanics Institute*, Stanford University Press, Stanford, Calif., 1965.

[3] Bower, W. W. and Incropera, F. P., "Heat Transfer, Development Length and Friction Factor Correlations for the Asymptotic Region of a Laminar Arc Constrictor," *Wärme- und Stoffübertragung*, Vol. 2, 1969, pp. 150–162.

[4] Bott, J. F., "Spectroscopic Measurement of Temperature in an Argon Arc Plasma," *The Physics of Fluids*, Vol. 9, No. 8, Aug. 1966, pp. 1540–1547.

[5] Giannaris, R. J. and Incropera, F. P., "Nonequilibrium Effects in

an Atmospheric Arc Plasma," *Journal of Quantitative Spectroscopy and Radiative Transfer*, Vol. 11, No. 2, Feb. 1971, pp. 291–307.

[6] Lukens, L. A. and Incropera, F. P., "Electric Field Intensity and Wall Heat Transfer Measurements for the Heating Region of an Atmospheric Cascade Arc," *International Journal of Heat and Mass Transfer*, Vol. 15, No. 5, May 1972, pp. 935–952.

[7] Uhlenbusch, J., Fischer, E., and Hackmann, J., "Untersuchungen von Nichtgleichgewichtseffekten an stationären Heliumplasmen," *Zeitschrift für Physik*, Vol. 238, No. 2, Feb. 1970, pp. 404–420.

[8] Kruger, C. H., "Nonequilibrium in Confined-Arc Plasmas," *The Physics of Fluids*, Vol. 13, No. 7, July 1970, pp. 1737–1746.

[9] Incropera, F. P. and Viegas, J. R., "Nonequilibrium in an Arc Constrictor," *AIAA Journal*, Vol. 8, No. 9, Sept. 1970, pp. 1722–1724.

[10] Clark, K. J. and Incropera, F. P., "Thermochemical Nonequilibrium in an Argon Constricted Arc Plasma," *AIAA Journal*, Vol. 10, No. 1, Jan. 1972, pp. 17–18.

[11] Scott, R. K., "Thermochemical Nonequilibrium in Atomic Hydrogen at Elevated Temperatures," Rept. HTGDL-8, Dec. 1972, Purdue Univ., Lafayette, Ind.

[12] Devoto, R. S., "Transport Coefficients of Partially Ionized Hydrogen," *Journal of Plasma Physics*, Vol. 2, No. 4, Dec. 1968, pp. 617–631.

[13] Hinnov, E. and Hirschberg, J. G., "Electron-Ion Recombination in Dense Plasmas," *Physical Review*, Vol. 125, No. 3, Feb. 1962, pp. 795–801.

[14] Allen, C. W., *Astrophysical Quantities*, University of London, The Athlone Press, London, England, 1955.

[15] Petschek, H. and Byron, S., "Approach to Equilibrium Ionization Behind Strong Shock Waves in Argon," *Annals of Physics*, Vol. 1, 1957, pp. 270–315.

[16] Yos, J. M., "Transport Properties of Nitrogen, Hydrogen, Oxygen and Air to 30,000°K," Rept. RAD TM-63-7, 1963, AVCO Corp., Wilmington, Mass.

[17] Longmire, C. L., *Elementary Plasma Physics*, Interscience, New York, 1963.

[18] Wiese, W. L., Paquette, D. R., and Solarski, J. E., "Profiles of Stark-Broadened Balmer Lines in a Hydrogen Plasma," *Physical Review*, Vol. 129, Pt. 1, 1963, pp. 1225–1232.

[19] Morris, J. C. et al., "Evaluation of High Temperature Gas Transport Properties," CR-575, 1966, NASA.

[20] Steinberger, S., "Messung von Temperaturverteilungen im H_2—Kaskadenbogen bis 27,000°K," *Zeitschrift für Physik*, Vol. 223, 1969, pp. 1–18.

[21] Maecker, H., "Transport Properties in High Power Arcs," ARL 69-0031, 1969, Aerospace Research Labs., Wright-Patterson Air Force Base, Ohio.

[22] Greene, C. S., "Parametric Calculations for the Asymptotic Region of Hydrogen, Helium, Argon, Krypton and Xenon Laminar Constricted Arcs," M.S. thesis, 1972, Purdue Univ., Lafayette, Ind.

DECEMBER 1973 AIAA JOURNAL VOL. 11, NO. 12

Starting Transient of Solid-Propellant Rocket Motors with High Internal Gas Velocities

A. PERETZ,* K. K. KUO,† L. H. CAVENY,‡ AND M. SUMMERFIELD§
Guggenheim Laboratories, Princeton University, Princeton, N.J.

A comprehensive analytical model which considers time and space development of the flowfield in solid-propellant rocket motors with high volumetric loading density is described. The gas dynamics in the motor chamber is governed by a set of hyperbolic partial differential equations, that are coupled with the ignition and flame spreading events, and with the axial variation of mass addition. The flame spreading rate is calculated by successive heating-to-ignition along the propellant surface. Experimental diagnostic studies have been performed with a rectangular window motor (50 cm grain length, 5 cm burning perimeter and 1 cm hydraulic port diameter), using a controllable head-end gaseous igniter. Tests were conducted with AP composite propellant at port-to-throat area ratios of 2.0, 1.5, 1.2, and 1.06, and head-end pressures from 35 to 75 atm. Calculated pressure transients and flame spreading rates are in very good agreement with those measured in the experimental system.

Nomenclature

A_p = cross-sectional area of the port, cm^2
A_t = motor nozzle throat area, cm^2
a = pre-exponential factor in the nonerosive burning rate law, ap^n
b = burning perimeter, cm
c = speed of sound, cm/sec; when with subscript, specific heat, cal/g-°K
c_p = specific heat at constant pressure, cal/g-°K
d_h = hydraulic diameter of the port, cm
E = total stored energy, cal/g
f = friction coefficient, $2g\tau_w/\rho u^2$
g = acceleration of gravity, conversion factor, g-cm/gf-sec^2¶
h_c = local convective heat-transfer coefficient, cal/cm^2-sec-°K
h_{cp} = local convective heat-transfer coefficient over the propellant surface, cal/cm^2-sec-°K
h_{cw} = local convective heat-transfer coefficient over nonpropellant port wall, cal/cm^2-sec-°K
h_f = enthalpy of combustion gas at adiabatic flame temperature, cal/g
h_p = port height (see Fig. 3), cm
J_c = mechanical equivalent of heat, gf-cm/cal
k = erosive burning constant, cm^3-°K/cal
L^* = characteristic length, cm
m_{ig} = igniter mass flow rate, g/sec

Presented as Paper 72-1119 at the AIAA/SAE 8th Joint Propulsion Specialist Conference, New Orleans, La., November 29–December 1, 1972; submitted December 14, 1972; revision received May 25, 1973. Based on work performed under NASA. Grant NGL 31-001-109 monitored by NASA Langley Research Center and the Jet Propulsion Laboratory of the California Institute of Technology.

Index categories: Combustion Stability, Ignition, and Detonation; Solid and Hybrid Rocket Engines; Nozzle and Channel Flow.

* Ph.D. Candidate. Member AIAA.

† Post-Doctoral Research Associate; presently Assistant Professor, Pennsylvania State University, University Park, Pa. Member AIAA.

‡ Senior Member of Professional Staff. Associate Fellow AIAA.

§ Professor of Aerospace Propulsion. Fellow AIAA.

¶ gf denotes unit of gram force.